NeuroImage 262 (2022) 119549

Contents lists available at ScienceDirect

NeuroImage

journal homepage: www.elsevier.com/locate/neuroimage

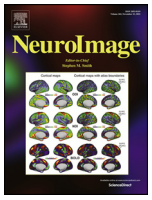

Multisensory integration of anticipated cardiac signals with visual targets affects their detection among multiple visual stimuli

Qiaoyue Ren, Amanda C. Marshall, Jakob Kaiser, Simone Schütz-Bosbach*

Department of Psychology, General and Experimental Psychology Unit, LMU Munich, Germany

ARTICLE INFO

Keywords:
Multisensory integration
Interoception
Visual search
Cardiac signals
Cardiac systole
Cardiac diastole

ABSTRACT

Many studies have elucidated the multisensory processing of different exteroceptive signals (e.g., auditory-visual stimuli), but less is known about the multisensory integration of interoceptive signals with exteroceptive information. Here, we investigated the perceptual outcomes and electrophysiological brain mechanisms of cardio-visual integration by using participants' electrocardiogram signals to control the color change of a visual target in dynamically changing displays. Reaction times increased when the target change coincided with strong cardiac signals concerning the state of cardiovascular arousal (i.e., presented at the end of ventricular systole), compared to when the target change occurred at a time when cardiac arousal was relatively low (i.e., presented at the end of ventricular diastole). Moreover, the concurrence of the target change and cardiac arousal signals modulated the event-related potentials and the beta power in an early period (~100 ms after stimulus onset), and decreased the N2pc and the beta lateralization in a later period (~200 ms after stimulus onset). Our results suggest that the multisensory integration of anticipated cardiac signals with a visual target negatively affects its detection among multiple visual stimuli, potentially by suppressing sensory processing and reducing attention toward the visual target. This finding highlights the role of cardiac information in visual processing and furthers our understanding of the brain dynamics underlying multisensory perception involving both interoception and exteroception.

1. Introduction

At any given moment, we receive inputs from various sensory modalities. The processes involved in integrating these multisensory inputs are fundamental to effective perception and cognitive functioning (Wallace et al., 2020). Past work on multisensory/cross-modal integration has largely focused on sensory inputs from the external world, i.e., exteroceptive signals such as visual and auditory stimuli (Tang et al., 2016; van Atteveldt et al., 2014). For example, an auditory signal co-occurring with a visual stimulus has been shown to facilitate visual detection (Leo et al., 2008), visual discrimination (Noesselt et al., 2008), and visual target search (Van der Burg et al., 2008, 2011). Auditory-visual integration starts as early as about 50 ms after stimulus onset (Giard and Peronnet, 1999; Molholm et al., 2002; Senkowski et al, 2011) and appears to modulate the activation of sensory cortices (Kayser et al., 2017; Martuzzi et al., 2007).

Recent neuroscientific research is progressively targeting interoceptive information from internal visceral organs (especially the heart) as an important source of sensory input for perceptual and cognitive processes in the brain (Chen et al., 2021; Park and Blanke, 2019; Quigley et al., 2021). Cardiac activity occurs in a cycle of two phases. During the ventricular systole, the muscles in the ventricle contract, pumping blood from the heart to the body. During the ventricular diastole, the heart muscle is relaxed as it refills with blood (DeSaix et al., 2018). It has been proposed that cardiac interoceptive information is conveyed to brain regions (e.g., the insula, cingulate cortex, amygdala, and somatosensory cortex) mainly by arterial baroreceptors located in the aortic arch and the carotid arteries (Azzalini et al., 2019; Garfinkel and Critchley, 2016; Park and Blanke, 2019). Within a cardiac cycle, these baroreceptors fire maximally at the end of ventricular systole and minimally at the end of ventricular diastole in response to the fluctuations of arterial blood pressure. In other words, cardiac signals are strongest at the end of the ventricular systole while relatively weak at the end of the ventricular diastole. In addition, heartbeats can evoke heartbeat evoked potentials (HEP) on the cortex, just like visual stimuli can evoke visually evoked potentials (Park and Blanke, 2019). Abundant work has suggested that the HEP reflects the cortical processing of cardiac afferent signals and is therefore a reliable neurophysiological marker of cardiac interoception (Coll et al., 2021; Park et al., 2018; Petzschner et al., 2019).

Up to now, there is only limited evidence about the multisensory processing of exteroceptive visual signals in combination with interoceptive cardiac signals. Previous investigations mainly focused on the cardiac cycle effect on visual perception, i.e., whether participants' re-

* Corresponding author.
E-mail address: S.Schuetz-Bosbach@psy.lmu.de (S. Schütz-Bosbach).

https://doi.org/10.1016/j.neuroimage.2022.119549.
Received 16 February 2022; Received in revised form 29 July 2022; Accepted 4 August 2022
Available online 5 August 2022.

sponses to a visual stimulus were modulated by the timing of the stimulus with respect to their cardiac cycle. While past work failed to find any cardiac cycle effect on the detection of flashes (Elliott and Graf, 1972), the majority of previous studies highlighted a significant impact of cardiac phase on visual processing. For example, the presentation of visual stimuli at systole compared to diastole has been shown to influence reaction times towards these stimuli, with most studies finding prolonged reaction times during the systole (McIntyre et al., 2007; Sandman et al., 1977, but see also: Makowski et al. (2021). Processing visual stimuli presented at cardiac systole compared to diastole evoked smaller visual evoked potentials (Walker and Sandman, 1982) and resulted in reduced interference of visually distracting stimuli (Pramme et al., 2014, 2016). In addition, cardiac cycle effects have been found to be modulated by the emotional valence of the visual stimuli: while fearful faces were detected more easily and rated as more intense if presented at systole compared with diastole, the detection of neutral, disgusted, or happy faces was comparable across the two cardiac phases (Garfinkel et al., 2014). Given that cardiac signals are conveyed to the brain mainly during the cardiac systole rather than the diastole (Azzalini et al., 2019; Garfinkel and Critchley, 2016), it can be assumed that cardiac signals may influence the perception and neural processing of a simultaneous visual stimulus. This assumption is also supported by the finding that visual evoked potentials are enhanced when these images are synchronized with participants' heartbeats compared to when they are presented out of synchrony to participants' heartbeats (Ronchi et al., 2017). By measuring neural markers of cardiac processing such as the HEP and insula activity (Coll et al., 2021; Salomon et al., 2018), recent studies have further provided evidence about the interplay between cardiac processing and visual processing. For example, the amplitude of the pre-stimulus heartbeat-evoked potential positively predicts subsequent visual detection (Park et al., 2014). Additionally, contrary to the finding reported by Ronchi et al. (2017), Salomon et al. (2016) observed that visual stimuli presented at participants' cardiac frequency take longer to enter visual awareness and induce smaller activation in the insular cortex. Up to now, it is still unclear how simultaneously encountered cardiac signals and visual information are integrated into the brain. Moreover, previous studies mainly examined the influence of cardiac signals on the perception of a single visual stimulus, leaving out the question how cardio-visual integration can affect the competition among multiple visual stimuli.

Here, we employed a novel adaptation of the dynamic visual search task (Van der Burg et al., 2008, 2011) to investigate the multisensory integration of cardiac signals with a visual target in a dynamic cluttered environment, while recording the electrocardiogram (ECG) and electroencephalogram (EEG). Critically, the visual target changed its color either at a time when cardiac arousal signals were strongly present (i.e., at the end of ventricular systole) or when cardiac arousal was relatively low and thus did not provide a strong signal (i.e., at the end of ventricular diastole). Consistent with both recent reviews (Azzalini et al., 2019; Quigley et al., 2021) and empirical studies (Ronchi et al., 2017; Sel et al., 2017), we treated visual and cardiac signals as sensory input signals of equal relevance. At the behavioral level, we measured reaction times and accuracy rates. At the electrophysiological level, we explored the brain dynamics of cardio-visual integration from two different perspectives. The first perspective was to compare the electrophysiological responses to the bimodal cardio-visual stimulus (i.e., the concurrence of cardiac arousal signals and the target change) with the sum of the electrophysiological responses to the unimodal cardiac arousal signals and the unimodal visual stimulus (i.e., the target change). This comparison approach (i.e., the additive model) has been widely used in previous EEG studies to reveal early multisensory processes underlying auditory-visual integration (Senkowski et al., 2011; Talsma and Woldorff, 2005; Van der Burg et al., 2011; Zhao et al., 2020, 2018). In the present study, this approach was applied in analyses of both event-related potentials (ERPs) and neural oscillations. According to the additive model (Cappe et al., 2010; Senkowski et al., 2011; Talsma and Woldorff, 2005), electrophysiological responses to the simultaneous cardiac and visual input would be different from the sum of the cardiac and visual responses alone if multisensory integration occurred across cardiac processing and visual processing in the brain. Second, the lateralized presentation of the visual target in the visual field made it possible to compare the lateralized electrophysiological responses to the bimodal cardio-visual stimulus and the unimodal visual stimulus. We mainly focused on the lateralized N2pc component and alpha/beta oscillations, which are well-validated measures of the allocation of attention to lateralized visual stimuli (Bacigalupo and Luck, 2019; Bauer et al., 2012).

2. Materials and methods

2.1. Participants

Twenty-six participants (12 females; mean age: 25.46 ± 0.87 years; range: 20–38 years) took part in the present study for payment (9 € per h) or student credits. All participants reported normal or corrected-to-normal vision, no color blindness, no diagnosed heart-rhythm abnormalities, no present or past psychiatric or neurological disorders, and no current use of medication. Consent was obtained from all participants, and the procedures were approved by the local ethics committee at the Department of Psychology of LMU Munich in accordance with the Declaration of Helsinki. To the best of our knowledge, no previous studies have explored cardio-visual integration in a similar task. Therefore, we could not compute the required sample size a priori. However, our sample size is comparable with relevant previous studies (e.g., Adelhöfer et al. 2020; Marshall et al. 2022; Pramme et al. 2016).

2.2. Experiment design

Participants completed a dynamic visual search task in which a display of randomly oriented line segments changed color dynamically (Van der Burg et al., 2008). Each display consisted of several oblique lines (the distractors), and only one line which was perfectly horizontal or vertical (the target). The participants had to identify the target as quickly as possible by indicating if it was horizontal or vertical via button press. To investigate the cardio-visual integration, the experiment contained two conditions in which the visual target changed color when cardiac arousal signals were relatively low (i.e., when arterial baroreceptors are relatively quiescent; corresponding to the end of ventricular diastole) or strong (i.e., when arterial baroreceptors fire strongly; corresponding to the end of ventricular systole; see Fig. 1A). The ventricular systole refers to the period from approximately the ECG R-peak to the T wave, and the ventricular diastole refers to the period from approximately the T wave to the next upcoming R-peak (DeSaix et al., 2018). In the diastole coupling condition, the color change of the visual target was designed to always occur at the R-peak to coincide with the end of ventricular diastole. In the systole coupling condition, the color change of the visual target was designed to always occur at 290 ms after the R-peak (approximately at the T wave) to coincide with the end of ventricular systole (Rae et al., 2020, 2018). Participants completed 10 diastole coupling blocks and 10 systole coupling blocks presented in counterbalanced, alternating order and preceded by 1 practice block. Each block consisted of 24 trials. In addition to the 20 blocks for the visual search task, one resting block (duration: 2.5 min) was performed before the task. During the resting block, participants were asked to look at the fixation dot centrally presented on the monitor while no other visual stimuli were presented. The EEG signal obtained from this type of resting condition has been used to correct for cardiac cycle-related artifacts present in the EEG signal of task conditions in previous studies (Ronchi et al., 2017; van Elk et al., 2014).

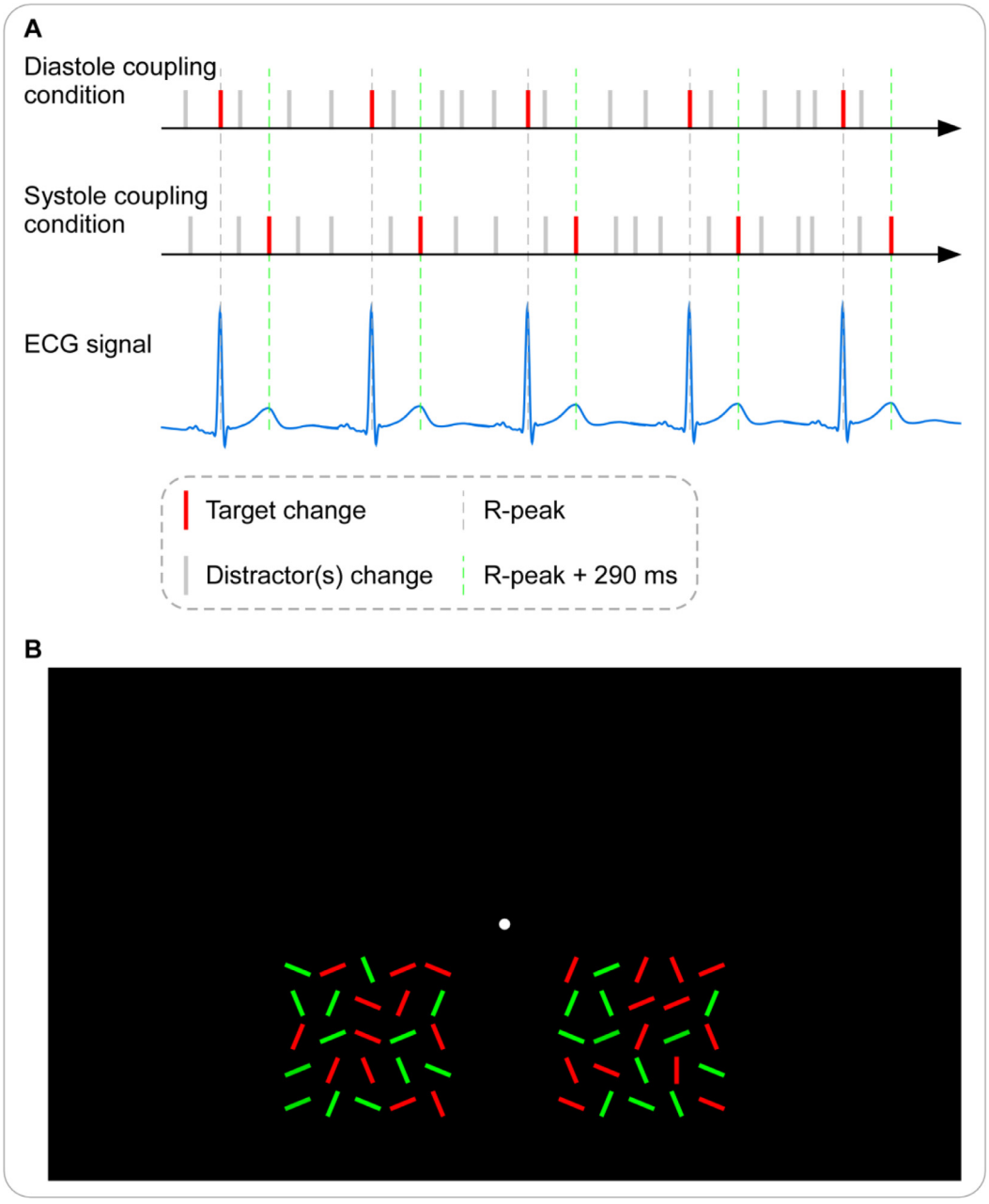

Fig. 1. The dynamic visual search task. (A) Schematic illustration of the experimental conditions. In the diastole coupling condition, the color change of the visual target always occurred at the R-peak to coincide with the end of ventricular diastole (i.e., when cardiac arousal signals were relatively low). In the systole coupling condition, the color change of the visual target always occurred at 290 ms after the R-peak to coincide with the end of ventricular systole (i.e., when cardiac arousal signals were strong). (B) An example visual search display. The search display consisted of 1 target (horizontal or vertical) and 49 distractors (oblique). In the example display, the target consists of the vertical red line on the right side. The colors of the target and the distractors (green or red) were randomly assigned and changed randomly over time. Participants were required to indicate the orientation of the visual target as fast and accurately as possible.

2.3. Stimuli and procedure

Participants were seated in a dimly lit room at 70 cm from the monitor (24 inches; refresh rate: 60 Hz; resolution: 1920 × 1080 pixels) with their heads on a chin rest. The visual search displays were generated and displayed using the Presentation software (Neurobehavioral Systems, Inc.).

Each search display consisted of 50 red (luminance: 49.5 cd/m^2) or green (49.5 cd/m^2) line segments on a black (0.30 cd/m^2) background (Fig. 1B). One of the line segments was the target, while the remaining ones acted as distractors. The color of each line segment was randomly determined. The target was either horizontal (visual angle: 0.60° × 0.10°) or vertical (0.10° × 0.60°). Each distractor was the same size as the target, but its orientation deviated randomly by either plus or minus 22.5° from horizontal or vertical. Given that target-elicited lateralized effects (e.g., N2pc component) are largely absent for upper-field visual targets (Bacigalupo and Luck, 2019), we presented the search display only in the lower visual field. Specifically, half of the line segments were placed on an invisible 5 × 5 grid (3.40° × 3.40°) in the lower left visual field, and the other half were placed on an identical grid in the lower right visual field. Both grids were 2.83° horizontally away from and 2.13° below the center of the screen marked with a white (245.00 cd/m^2) fixation dot. To avoid immediate target detection after the search display appeared, the target never appeared on the outer ring

of each grid (Van der Burg et al., 2011). Target orientation (horizontal or vertical) and location (left or right visual field) were balanced and randomly mixed within blocks.

In order to time-lock the target rather than the distractors to specific time points in each cardiac cycle, the search display changed continuously by switching the color of a random number of line segments between red and green (i.e., either from red to green or from green to red). Color changes of either the target or the distractors never occurred at the same time. That is, at a given moment either the target changed its color while the color of the distractors remained unchanged, or some of the distractors changed their color while the target's color remained constant. During each distractor change, we switched the color of either one, four, or seven randomly selected line segments. The interval between two successive color changes in the visual display varied randomly from 50 to 250 ms. However, there were two constraints with respect to the timings of the color changes. First, the visual target could change its color only once in each cardiac cycle, either at the R-peak (in the diastole coupling condition) or 290 ms after the R-peak (in the systole coupling condition). Second, the distractors could never change within the time window from -150 to 100 ms relative to the two aforementioned timings specific for the target change, to promote unambiguous binding of the target change and cardiac signals (Van der Burg et al., 2008, 2011). In other words, the distractors could change color within the time window from 100 to 140 ms after the R-peak and within the time window from 390 ms after the R-peak to 150 ms before the next R-peak in both coupling conditions. In this way, we ensured that the timings of distractor color changes were comparable across the two cardiac coupling conditions and thus would not lead to any confounding effect. The onset of an upcoming R-peak was estimated by calculating a median inter-beat interval based on the timings of the previous six R-peaks.

Each trial started with a central fixation dot, followed by a dynamic visual search display. The onset of the search display was randomly set from 0 to 600 ms after the R-peak to avoid it coinciding with specific time points in the cardiac cycle. Notably, it was the first R-peak detected 800 ms after the onset of the fixation dot that was used to calculate the onset of the search display. This ensured that the presentation of the fixation dot was not too short, i.e., at least 800 ms. The search display remained on the screen until the participant responded or the visual target had changed five times (i.e., 5 heartbeats, about 4000 ms). Note that in the latter case, the search display would not disappear immediately but disappear 300 ms after the fifth target change to ensure that the fifth target change was perceivable. Participants were asked to indicate the visual target orientation as fast and accurately as possible by a button press ("F" and "J" corresponding to horizontal and vertical, respectively). At the end of each trial, there was a blank presented for 1000 ms. Participants were required to maintain fixation of the central dot during the trial and try to blink only during the breaks. Accuracy rate and mean reaction time were presented as visual feedback after each block during the self-paced inter-block rest.

2.4. Recordings

For EEG recording, we used 65 active electrodes (BrainProducts ActiSnap) and 1 additional ground electrode positioned following the international 10–20 system. The FCz functioned as the online reference for these scalp electrodes. Horizontal and vertical electrooculograms (EOGs) were also recorded via electrodes at the left and right outer canthi, and electrodes above and below the left eye, respectively. For recording ECG, we used 3 electrodes placed below the left clavicle (reference electrode), the right clavicle (ground electrode), and the left pectoral muscle (active electrode) respectively. All impedances were kept below 20 kΩ. Both EEG and ECG were recorded using a 1000 Hz sampling rate and a 0.1–1000 Hz online bandpass filter. Signal acquisition and amplification were implemented using the BrainVision Recorder software (Brain Products, Inc.). Online detection of the ECG R-peaks was achieved using the BrainVision RecView software (Brain Products, Inc.). ECG R-peaks were defined as the first decreasing voltage sample after exceeding a constant threshold. The threshold was individually set after the experimenter visually inspected the 2.5 min ECG signal during the resting block. Each detection of the R-peak added a marker to the online ECG signals and sent a pulse to the experimental PC. During the experiment, the pulse-related markers were visually inspected by the experimenter to ensure that R-peaks were detected with high precision. Furthermore, a post hoc analysis was performed to check the precision of the R-peak detection and the latencies between the ECG R-peaks and the visual stimuli (i.e., the color changes of the visual target) across the experiment. Specifically, we used the NeuroKit2 toolbox (Makowski et al., 2021) in Python to identify the timings of the R-peaks in the offline ECG data, and then compared them with the timings of the target changes. The results suggest that we detected the R-peaks in real-time ECG signal with high precision (in the diastole coupling condition: hit rate: 92.35 ± 1.48%; missing rate: 7.65 ± 1.48%; false alarm rate: 4.13 ± 1.02%; in the systole coupling condition: hit rate: 90.09 ± 2.11%; missing rate: 9.91 ± 2.11%; false alarm rate: 3.37 ± 0.78%), and that the target changes were time-locked to R-peaks (in the diastole coupling condition: 120.78 ± 8.51 ms after R-peaks) or 290 ms after R-peaks (in the systole coupling condition: 403.25 ± 6.57 ms after R-peaks) accordingly in close temporal proximity.

2.5. Behavioral analysis

Behavioral performance was assessed by reaction times for correct responses and accuracy rates in the diastole coupling and the systole coupling condition. Notably, although the number of distractors per display (i.e., 49) was relatively large to avoid immediate visual target detection, in a minority of trials (8.12 ± 1.96% and 2.50 ± 0.75% of diastole coupling and systole coupling trials per participant, respectively), participants found the visual target very fast and responded before the first color change of the visual target. These trials were excluded in the behavioral analysis as the experimental manipulation could not be effective (i.e., coupling the color change of the visual target to the presence of strong or weak cardiac signals).

2.6. EEG Preprocessing

EEG data were preprocessed using MATLAB toolbox FieldTrip (Oostenveld et al., 2011). EEG data were re-referenced to the common average, filtered using a 40 Hz low-pass filter, and down-sampled to 500 Hz. No bad electrodes were found. Then, EEG epochs were extracted between -800 and 900 ms around the color change of the visual target. Independent component analysis (ICA) was conducted to identify stereotypical components reflecting eye movements, blinks, and the cardiac field artifact (CFA) which is produced by the movement of the heart muscle. The eye-related artifactual components were manually identified and removed based on scalp topography and time course (2.42 ± 0.32 components per participant), while CFA-related components were identified using a custom algorithm. More specifically, we first redefined EEG trials around the ECG R-peaks. Then, we computed the coherence of the time-frequency data between each independent component and the ECG signal, and elected four components with the highest coherence. Finally, we decided which of the four components should be removed (1.50 ± 0.21 components per participant) based on additional characteristics which were commonly associated with CFA, e.g., a bimodal topography, a frequency peak around 5 Hz, and a rhythmically repeating time course (Viola et al., 2009). Furthermore, epochs contaminated by artifacts (e.g., eye movements and muscle activity) were automatically rejected based on a threshold of four times the standard deviation in the horizontal EOG channel and a threshold of ± 100 μV in EEG channels.

In total, 14.12 ± 2.25% of trials per participant were rejected due to (i) lack of target change before the participant responded, and (ii)

the contamination of artifacts. Additionally, only trials with correct responses were included in further EEG analysis. These procedures left on average 168.42 ± 7.97 trials for the diastole coupling condition and 155.04 ± 5.76 trials for the systole coupling condition per participant.

2.7. ERP analysis

EEG epochs were further segmented into periods ranging from -100 to 600 ms relative to four events of interest, with baseline correction using the first 100 ms period. Specifically, in the diastole coupling condition (i.e., time-locking the target change to the R-peak), we assumed that the epochs time-locked to the target change (i.e., about at the R-peak) mainly reflected the responses to the visual stimulus (i.e., unimodal visual input as in this situation the cardiac arousal was low and the visual stimulus therefore was assumed to provide the dominant sensory input). Whereas, the epochs timed-locked to 290 ms after the target change (i.e., about at 290 ms after the R-peak) were assumed to mainly reflect the responses to cardiac signals (i.e., unimodal cardiac input as in this situation no visual stimulus was changing color but the cardiac signals were strong and therefore were assumed to provide the dominant sensory input). In the systole coupling condition (i.e., time-locking the target change to 290 ms after the R-peak), we assumed that the epochs time-locked to the target change (i.e., about at 290 ms after the R-peak) reflected the responses to not only the visual stimulus but also the concurrent cardiac signals (i.e., bimodal input as the sensory input was a combined cardio-visual stimulus). Whereas, the epochs time-locked to 290 ms before the target change (i.e., about at the R-peak) were assumed to reflect the responses to “no stimulus” (i.e., at this moment the cardiac arousal was low and no visual stimulus was changing color). We referred to this condition as "no stimulus" as it did not include any stimulus-evoked EEG responses of interest (i.e., EEG responses evoked by the cardiac signals, the visual target, or the cardio-visual stimulus), which helps to distinguish it from the other three conditions including the EEG responses of interest.

Altogether, this procedure yielded four kinds of epochs time-locked to the unimodal visual stimulus, the unimodal cardiac signals, the bimodal cardio-visual stimulus, and the “no stimulus”, respectively (Supplementary Fig. 1). Please note that we used the term “unimodal” to empathize that the brain receives relevant sensory input mainly from a single modality (i.e., the cardiac modality or the visual modality) at a given moment, and that we use “bimodal” to empathize that the brain simultaneously receives relevant sensory information from two different modalities (i.e., the cardiac modality and the visual modality) at a given moment. In addition, as visual-evoked responses could generally last over 500 ms (Fong et al., 2020), all four kinds of epochs also included residual distractor evoked responses. However, any residual distractor evoked responses had been removed prior to comparisons of the relevant experimental conditions and could thus not affect the results in the present study (see detailed explanation in Section 2.9).

2.8. Time-frequency analysis

EEG epochs were decomposed into their time-frequency representations using Morlet wavelets (Tallon-Baudry and Bertrand, 1999) from 2 to 40 Hz in steps of 1 Hz (Kaiser and Schütz-Bosbach, 2021). The number of wavelet cycles increased from 3 to 10 cycles in linearly spaced steps to have a good balance between time and frequency resolution. Consistent with the ERP analysis, time-frequency data were further segmented into periods ranging from -300 to 500 ms relative to the four events of interest (i.e., the unimodal visual stimulus, the unimodal cardiac signals, the bimodal cardio-visual stimulus, and the “no stimulus”), with baseline correction via decibel conversion using the period from -300 to -100 ms. This baseline interval was chosen to avoid the adverse influence of spectral estimates biased by windowing post-stimulus activity and padding values (Hu and Zhang, 2019; Zhang et al., 2020).

2.9. Statistical analysis

For behavioral data, separate paired samples *t*-tests were performed to compare reaction times and accuracy rates between the diastole coupling and the systole coupling condition. The effect size was estimated by Cohen’s *d*.

For ERP data, to investigate the cardio-visual integration in early sensory processing, the ERP elicited by the bimodal cardio-visual stimulus was compared with the summed ERP elicited by the unimodal cardiac signals and visual stimulus. Consistent with previous studies (Senkowski et al., 2011; Talsma and Woldorff, 2005; Van der Burg et al., 2011), the average waveform time-locked to the “no stimulus” was subtracted from the original waveforms elicited by the bimodal cardio-visual stimulus, the unimodal cardiac signals, and the unimodal visual stimulus, respectively, to correct for any residual distractor evoked responses. While we expect an early cardio-visual interaction (< 200 ms; Giard and Peronnet, 1999; Van der Burg et al., 2011; Zhao et al., 2020), we did not have a clear prediction regarding the morphology (latency and topography) of this effect. Therefore, a nonparametric cluster-based permutation *t*-test (the responses to the bimodal cardio-visual stimulus versus the summed responses to the unimodal cardiac signals and visual stimulus) was applied for the ERP amplitudes in the time window from 0 to 200 ms relative to the stimulus onset.

In addition, to investigate the cardio-visual integration in visuospatial selective attention, we compared the N2pc components elicited by the bimodal cardio-visual stimulus and by the unimodal visual stimulus. The N2pc components were measured by the contralateral-minus-ipsilateral difference waveforms relative to the side of the visual target (left or right visual field). Please note that a correction of residual distractor evoked responses prior to this analysis was not required, as the color change of distractors randomly occurred in both visual fields and thus, contralateral-minus-ipsilateral EEG responses were not affected by any residual distractor evoked responses. Previous studies consistently found the maximum N2pc amplitude in the time window from 200 to 300 ms relative to the stimulus onset and around the lateral posterior electrodes (Arslanova et al., 2019; Luck and Hillyard, 1994; Van der Burg et al., 2011). Therefore, a nonparametric cluster-based permutation *t*-test was applied for N2pc amplitudes in this time window and electrode region (left hemisphere: P3, P7, O1, P1, P5, PO7, and PO3; right hemisphere: P4, P8, O2, P2, P6, PO8, and PO4).

For time-frequency data, to investigate the cardio-visual integration in neural oscillations related to early sensory processing, the oscillation power elicited by the bimodal cardio-visual stimulus was compared with the summed oscillation power elicited by the unimodal cardiac signals and visual stimulus. Notably, the time-frequency maps time-locked to the bimodal cardio-visual stimulus, the unimodal cardiac signals, the unimodal visual stimulus, and the “no stimulus” were first averaged over a cluster of posterior electrodes (CP5, P7, P5, P3, P1, PO7, POz, PO4, P4, Oz), respectively. These electrodes were chosen to match the electrodes revealing a prominent early cardio-visual interaction in the ERP analysis. Then, consistent with the ERP analysis, the average oscillation power time-locked to the “no stimulus” was subtracted from the original oscillation power elicited by the bimodal cardio-visual stimulus, the unimodal cardiac signals, and the unimodal visual stimulus, respectively, to correct for potential residual distractor evoked responses. Finally, a nonparametric cluster-based permutation *t*-test (responses to the bimodal cardio-visual stimulus versus the summed responses to the unimodal cardiac signals and visual stimulus) was applied to determine oscillatory power in the time window from 0 to 300 ms relative to the stimulus onset and in frequencies from 2 to 40 Hz.

In addition, to investigate the cardio-visual integration in neural oscillations related to visuospatial selective attention, we compared the lateralized oscillation power elicited by the bimodal cardio-visual stimulus and by the unimodal visual stimulus. The lateralized oscillation power was measured by the contralateral-minus-ipsilateral difference time-frequency maps relative to the side of the visual target (left or

right visual field). A correction of residual distractor evoked responses prior to this analysis was again not required, as the color change of distractors randomly occurred in both visual fields and thus, contralateral-minus-ipsilateral EEG responses were not affected by any residual distractor evoked responses. Notably, the contralateral-minus-ipsilateral difference time-frequency maps time-locked to the cardio-visual stimulus and the visual stimulus were first averaged over a cluster of lateral posterior electrodes (left hemisphere: P5, PO7, P3; right hemisphere: P6, PO8, P4), respectively. These electrodes were chosen to match the electrodes revealing a prominent cardio-visual interaction in the N2pc analysis. Then, a nonparametric cluster-based permutation *t*-test was applied for the lateralized oscillation power in the time window from 100 to 400 ms relative to the stimulus onset and in frequencies from 2 to 40 Hz.

Nonparametric cluster-based permutation *t*-tests were performed using the FieldTrip toolbox (Oostenveld et al., 2011). Permutation analysis allows for statistical tests over whole time series or time-frequency maps, while still controlling for multiple comparisons (Maris and Oostenveld, 2007). More specifically, for each permutation test used in the present study, adjacent spatio-temporal or spatio-spectro-temporal points for which *t*-values exceed a threshold were clustered (dependent *t*-test; cluster-defining threshold $p = .05$, two-tailed; iterations = 5000). Then, the cluster-level statistics were calculated by taking the sum of the *t*-values of all points within each cluster. Last, the observed cluster-level statistic was compared against the permutation distribution to test the null hypothesis of no difference between conditions (two-tailed test). Clusters with $p < .05$ were considered significant.

Unlike the *p*-value in frequentist hypothesis testing, the Bayes Factors (e.g., the BF_{10} value) in Bayesian hypothesis testing can indicate how much more likely the alternative hypothesis is than the null hypothesis (Wagenmakers et al., 2018). Therefore, for all the tests in behavioral and EEG analyses, we also reported BF_{10} values from the corresponding Bayesian tests performed in the JASP software (JASP Team, 2022). For the *t*-tests, in the absence of previous evidence on cardio-visual integration, we used the default priors, which assume a medium effect size on a Cauchy distribution of 0.707. A BF_{10} between 1.00 and 3.00 was interpreted as an anecdotal effect, a BF_{10} between 3.00 and 10.00 as a moderate effect, and a BF_{10} greater than 10.00 as a strong effect (Wagenmakers et al., 2018).

2.10. Control analyzes to exclude possible effects of cardiovascular artifacts

Cardiac cycle-related EEG responses include not only neural responses evoked by cardiac signals but also cardiac field artifact and pulse-related artifact (Kern et al., 2013). Any potential effects of cardiac cycle-related artifacts on our results should thus be carefully considered. We therefore conducted two sets of control analyses to ensure that the observed effects in the present study are caused by neural responses rather than cardiac cycle-related artifacts.

The first set of control analyses was inspired by Petzschner et al. (2019). To rule out any impact of cardiac cycle-related artifacts on the effect in early ERP amplitude, firstly, we compared the mean ECG amplitudes and the mean heart rates within the time window (46–142 ms) of this effect between the bimodal cardio-visual stimulus condition and the unimodal cardiac signals + unimodal visual stimulus condition, using separate paired samples *t*-tests. Secondly, we tested if there was any relationship between the differences in early ERP amplitude and the differences in ECG amplitude as well as the differences in heart rate across the aforementioned two conditions using separate linear regressions, i.e., predict the differences in early ERP amplitude from the differences in ECG amplitude or from the differences in heart rate across participants. Furthermore, we also compared the heart rates at R-peak between the systole coupling condition and the diastole coupling condition, and we tested if there was any relationship between the differences in early ERP amplitude across the bimodal cardio-visual stimulus condition and the unimodal cardiac signals + unimodal visual stimulus condition and the differences in the heart rate at R-peak across the two coupling conditions, using linear regression. The heart rate at each R-peak and the heart rate at each time point were calculated based on ECG signal using the NeuroKit2 toolbox (Makowski et al., 2021).

Similarly, to rule out any impact of cardiac cycle-related artifacts on the effect in early upper-alpha/beta power, firstly, we compared the mean ECG power and the mean heart rates within the time window (60–300 ms) and frequency window (11–24 Hz) of this effect between the bimodal cardio-visual stimulus condition and the unimodal cardiac signals + unimodal visual stimulus condition, using separate paired samples *t*-tests. Secondly, we tested if there was any relationship between the differences in early EEG power and the differences in ECG power as well as the differences in heart rate across the aforementioned two conditions using separate linear regressions, i.e., predict the differences in EEG power from the differences in ECG power or from the differences in heart rate across participants. We also tested if there was any relationship between the differences in early EEG power across the bimodal cardio-visual stimulus condition and the unimodal cardiac signals + unimodal visual stimulus condition and the differences in the heart rate at R-peak across the two coupling conditions, using linear regression.

However, this approach does not allow exploring the impact of cardiac cycle-related artifacts on the effects in lateralized N2pc amplitude and lateralized beta power, because it is impossible to extract lateralized ECG response from a single ECG channel. Moreover, the linear regression analysis can detect only potential linear but not nonlinear effects of cardiac cycle-related artifacts, and it does not consider any trial-by-trial variability.

We therefore performed another set of control analyses as suggested by some previous studies (Al et al., 2020; Gray et al., 2010; Ronchi et al., 2017; van Elk et al., 2014). Specifically, for each EEG epoch of our task conditions, we first calculated the latency between the event of interest and the previous ECG R-peak. Then we extracted EEG epochs timed-locked to the time point having identical latency after the R-peak during the resting condition, in which no visual stimulus was presented. Next, we averaged the epochs of the resting condition for each EEG electrode. Lastly, we subtracted the mean signal of the resting condition from the aforementioned epoch of the task conditions for each EEG electrode. The corrected EEG data was analyzed using the same statistical methods as the uncorrected data. That is, by using separate nonparametric cluster-based permutation *t*-tests, we (1) compared the ERP amplitude elicited by the bimodal cardio-visual stimulus with the summed ERP amplitude elicited by the unimodal cardiac signals and visual stimulus; (2) compared the N2pc amplitudes elicited by the bimodal cardio-visual stimulus and by the unimodal visual stimulus; (3) compared the oscillation power elicited by the bimodal cardio-visual stimulus with the summed oscillation power elicited by the unimodal cardiac signals and visual stimulus; (4) compared the lateralized oscillation power elicited by the bimodal cardio-visual stimulus and by the unimodal visual stimulus.

Please note that there is a caveat to this artifact correction approach. The epochs of the resting condition not only include cardiac cycle-related artifacts, but also neural responses evoked by cardiac signals, as they were time-locked to one specific time point within the cardiac cycle. Hence, this correction procedure not only removes cardiac cycle-related artifacts that we aimed to control for, but also (at least in part) cardiac cycle-related brain responses, that is, the EEG measures of interest in the present study. We therefore report both the uncorrected (see Section 3.2 and 3.3) and corrected data (see Section 3.4.3 and 3.4.4).

3. Results

3.1. Behavioural results

The paired samples *t*-tests showed that reaction times were prolonged in the systole coupling condition (2034.70 ± 108.40 ms), i.e.,

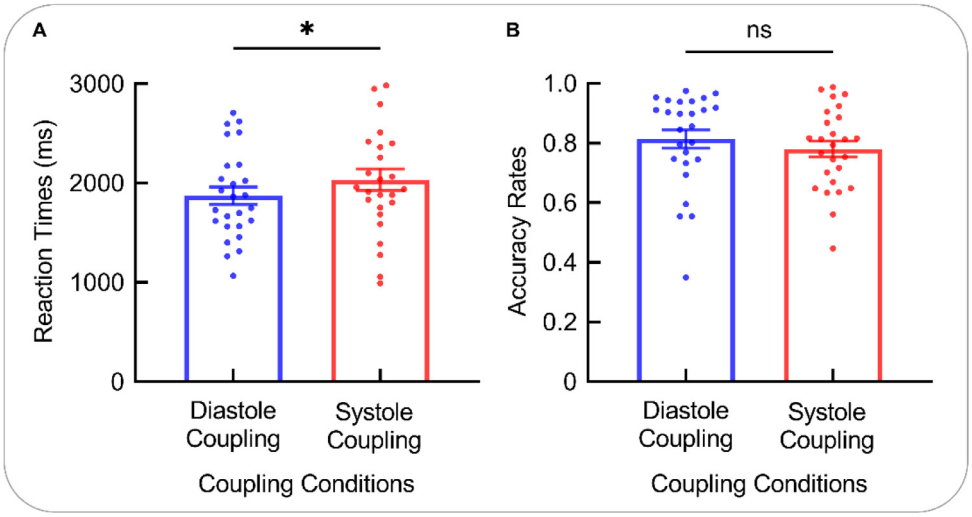

Fig. 2. Reaction times and accuracy rates. The reaction times were prolonged in the systole coupling condition, i.e., when the color change of the visual target coincided with strong cardiac signals concerning the state of cardiovascular arousal, compared to the diastole coupling condition, i.e., when the color change of the visual target occurred at a time when cardiac arousal was relatively low. However, the accuracy rates did not significantly differ between the two conditions. Data are expressed as M ± *SEM*. ns: not significant; *: $p < .05$.

when the color change of the visual target coincided with strong cardiac signals concerning the state of cardiovascular arousal, compared to the diastole coupling condition (1874.36 ± 87.61 ms), i.e., when the color change of the visual target occurred at a time when cardiac arousal was relatively low ($t(25) = 2.54$, $p = .017$, Cohen's $d = 0.50$, $BF_{10} = 2.96$). However, the accuracy rates did not significantly differ between the diastole coupling (0.81 ± 0.03) and the systole coupling condition (0.78 ± 0.03; $t(25) = -1.37$, $p = .182$, Cohen's $d = -0.27$, $BF_{10} = 0.48$). Fig. 2 represents the reaction times and accuracy rates in the diastole coupling and the systole coupling condition.

3.2. ERP results

3.2.1. Early cardio-visual integration in ERPs

The nonparametric cluster-based permutation *t*-test for ERP amplitudes revealed a significant cluster over posterior electrodes (CP5, P7, P5, P3, P1, PO7, POz, PO4, P4, and Oz; ~46–142 ms; $p = .023$, Cohen's $d = -0.77$). The ERP amplitude elicited by the bimodal cardio-visual stimulus (-1.22 ± 0.17 μV) was larger than the summed ERP amplitude elicited by the unimodal cardiac signals and visual stimulus (-0.87 ± 0.17 μV; $BF_{10} = 53.64$; see Fig. 3).

3.3. The effect of cardio-visual integration in lateralized N2pc components

The nonparametric cluster-based permutation *t*-test for contralateral-minus-ipsilateral N2pc amplitudes revealed a significant cluster over lateral posterior electrodes (left hemisphere: P5, PO7, and P3; right hemisphere: P6, PO8, and P4; ~220–246 ms; $p = .016$, Cohen's $d = 0.56$). Compared to the unimodal visual stimulus (-0.60 ± 0.10 μV), the bimodal cardio-visual stimulus elicited a lower N2pc amplitude (-0.26 ± 0.07 μV; $BF_{10} = 5.30$; see Fig. 4).

3.4. Time-frequency results

3.4.1. Early cardio-visual integration in oscillation power

The nonparametric cluster-based permutation *t*-test for oscillation power revealed a significant cluster within the upper-alpha/beta range (11–24 Hz; CP5, P7, P5, P3, P1, PO7, POz, PO4, P4, and Oz; ~60–300 ms; $p < .001$, Cohen's $d = -0.67$). The upper-alpha/beta power elicited by the bimodal cardio-visual stimulus (0.49 ± 0.12 dB) was lower than the summed upper-alpha/beta power elicited by the unimodal cardiac signals and visual stimulus (0.78 ± 0.17 dB; $BF_{10} = 16.75$; see Fig. 5).

3.4.2. The effect of cardio-visual integration in lateralized oscillation power

The nonparametric cluster-based permutation *t*-test for lateralized oscillation power revealed a significant cluster within the beta range (16–26 Hz; left hemisphere: P5, PO7, and P3; right hemisphere: P6, PO8, and P4; ~180–340 ms; $p = .006$, Cohen's $d = 0.93$). Compared to the unimodal visual stimulus (-0.20 ± 0.05 dB), the bimodal cardio-visual stimulus elicited weaker beta lateralization (0.07 ± 0.05 dB; $BF_{10} = 354.15$; see Fig. 6).

3.5. Results of control analyses to exclude possible effects of cardiovascular artifacts

3.5.1. No impact of ECG amplitude and heart rate on the effect in early ERP amplitude

Within the time window (46–142 ms) of the effect in early ERP amplitude, we did not find any relationship between the differences in early ERP amplitude and the differences in ECG amplitude across the bimodal cardio-visual stimulus condition and the unimodal cardiac signals + unimodal visual stimulus condition (linear regression: $F(1,25) = 1.97$, $p = .173$, $R^2 = .08$, $BF_{10} = 0.74$), although there was a significant difference between the ECG amplitude in response to the bimodal cardio-visual stimulus (96.42 ± 19.06 μV) and the summed ECG amplitude in response to the unimodal cardiac signals and visual stimulus (51.69 ± 22.09 μV; $t(25) = 6.49$, $p < .001$, Cohen's $d = 1.27$, $BF_{10} = 20736.45$; see Supplementary Fig. 1).

In addition, within the time window (46–142 ms) of the effect in early ERP amplitude, there was no difference between the heart rate in response to the bimodal cardio-visual stimulus (-0.08 ± 0.02 bpm) and the summed heart rate in response to the unimodal cardiac signals and visual stimulus (-0.05 ± 0.04 bpm; $t(25) = -0.77$, $p = .447$, Cohen's $d = -0.15$, $BF_{10} = 0.27$). We did not find any relationship between the differences in early ERP amplitude and the differences in heart rate across the bimodal cardio-visual stimulus condition and the unimodal cardiac signals + unimodal visual stimulus condition, either (linear regression: $F(1,25) = 3.23$, $p = .085$, $R^2 = .12$, $BF_{10} = 0.87$).

Furthermore, we did not find any relationship between the differences in early ERP amplitude across the bimodal cardio-visual stimulus condition and the unimodal cardiac signals + unimodal visual stimulus condition and the differences in heart rate at R-peak across the systole coupling condition and the diastole coupling condition (linear regression: $F(1,25) = 2.55$, $p = .123$, $R^2 = .10$, $BF_{10} = 0.91$), although there was a significant difference in heart rate between the systole coupling (74.82 ± 2.15 bpm) and the diastole coupling condition (73.76 ± 2.13 bpm; $t(25) = 2.43$, $p = .022$, Cohen's $d = 0.48$, $BF_{10} = 2.41$).

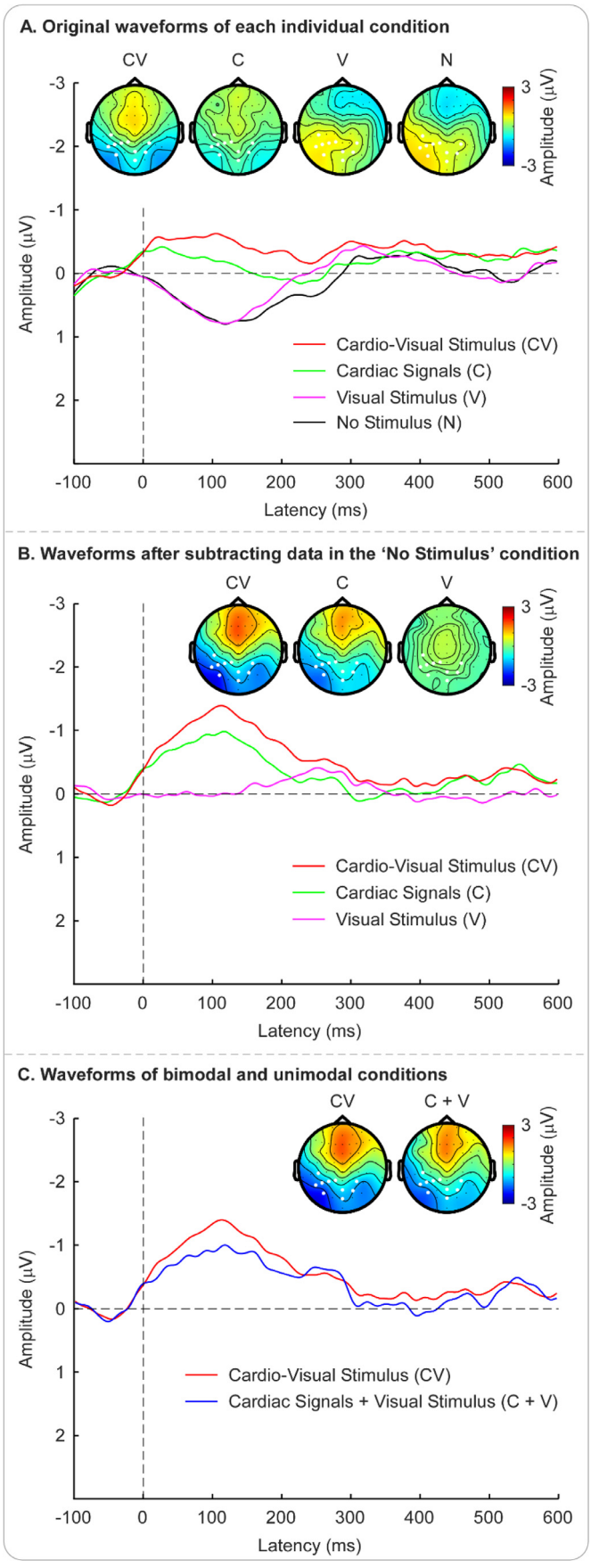

Fig. 3. Early cardio-visual integration in ERPs. (A) The original grand-average waveforms elicited by the bimodal cardio-visual stimulus, the unimodal cardiac signals, the unimodal visual stimulus, and the "no stimulus", respectively. Notably, the waveform elicited by the cardio-visual stimulus was time-locked to the target change in the systole coupling condition (about at 290 ms after the R-peak); the waveform elicited by the cardiac signals was time-locked to 290 ms after the target change in the diastole coupling condition (about at 290 ms after the R-peak); the waveform elicited by the visual stimulus was time-locked to the target change in the diastole coupling condition (about at the R-peak); the waveform elicited by the "no stimulus" was time-locked to 290 ms before the target change in the systole coupling condition (about at the R-peak). (B) The grand-average waveforms elicited by the bimodal cardio-visual stimulus, the unimodal cardiac signals, and the unimodal visual stimulus after subtraction of the waveform elicited by the "no stimulus", respectively. (C) The grand-average waveform elicited by the bimodal cardio-visual stimulus and the summed waveform elicited by the unimodal cardiac signals and visual stimulus. Permutation analysis indicated that the ERP amplitude elicited by the bimodal cardio-visual stimulus was larger than the summed ERP amplitude elicited by the unimodal cardiac signals and visual stimulus. This corresponded to a cluster extended from 46 to 142 ms after stimulus onset over posterior electrodes. Electrodes with high contribution to the cluster (i.e., with a total number of significant samples at or above the mean; CP5, P7, P5, P3, P1, PO7, POz, PO4, P4, and Oz) are highlighted with enlarged white dots in the scalp topographies.

3.5.2. No impact of ECG power and heart rate on the effect in early EEG power

Within the time window (60–300 ms) and frequency window (11–24 Hz) of the effect in early EEG power, we did not find any relationship between the differences in early EEG power and the differences in ECG power across the bimodal cardio-visual stimulus condition and the unimodal cardiac signals + unimodal visual stimulus condition (linear regression: $F(1,25) = 2.47$, $p = .129$, $R^2 = .09$, $BF_{10} = 0.88$), although there was a significant difference between the ECG power in response to the bimodal cardio-visual stimulus (25.27 ± 2.09 μV) and the summed ECG power in response to the unimodal cardiac signals and visual stimulus (27.56 ± 2.49 μV; $t(25) = -2.70$, $p = .012$, Cohen's $d = -0.53$, $BF_{10} = 4.01$; see Supplementary Fig. 2).

In addition, within the time window (60–300 ms) and frequency window (11–24 Hz) of the effect in early EEG power, we did not find any relationship between the differences in early EEG power and the differences in heart rate across the bimodal cardio-visual stimulus condition and the unimodal cardiac signals + unimodal visual stimulus condition (linear regression: $F(1,25) = 1.81$, $p = .191$, $R^2 = .07$, $BF_{10} = 0.70$), although there was a significant difference between the heart rate in response to the bimodal cardio-visual stimulus (-0.63 ± 0.11 bpm) and the summed heart rate in response to the unimodal cardiac signals and visual stimulus (-2.65 ± 0.92 bpm; $t(25) = 2.27$, $p = .032$, Cohen's $d = 0.45$, $BF_{10} = 1.81$).

Furthermore, we did not find any relationship between the differences in early EEG power across the bimodal cardio-visual stimulus condition and the unimodal cardiac signals + unimodal visual stimulus condition and the differences in heart rate at R-peak across the systole coupling condition and the diastole coupling condition (linear regression: $F(1,25) = 3.09$, $p = .092$, $R^2 = .11$, $BF_{10} = 0.91$). The scatter plots of linear regression are displayed in Supplementary Fig. 3.

3.5.3. ERP results based on corrected data

The nonparametric cluster-based permutation *t*-test for ERP amplitudes revealed a significant cluster over posterior electrodes (CP5, P7, P5, PO7, and P4; ~90–136 ms; $p = .046$, Cohen's $d = -0.78$). The ERP amplitude elicited by the bimodal cardio-visual stimulus (-0.51 ± 0.29 μV) was larger than the summed ERP amplitude elicited by the unimodal cardiac signals and visual stimulus (-0.08 ± 0.28 μV; $BF_{10} = 63.41$; see Supplementary Fig. 4).

The nonparametric cluster-based permutation *t*-test for contralateral-minus-ipsilateral N2pc amplitudes revealed a significant cluster over lateral posterior electrodes (left hemisphere: P5, PO7, and P3; right hemisphere: P6, PO8, and P4; ~220–250 ms; $p = .016$, Cohen's $d = 0.57$). Compared to the unimodal visual stimulus (-0.59 ± 0.10 μV), the

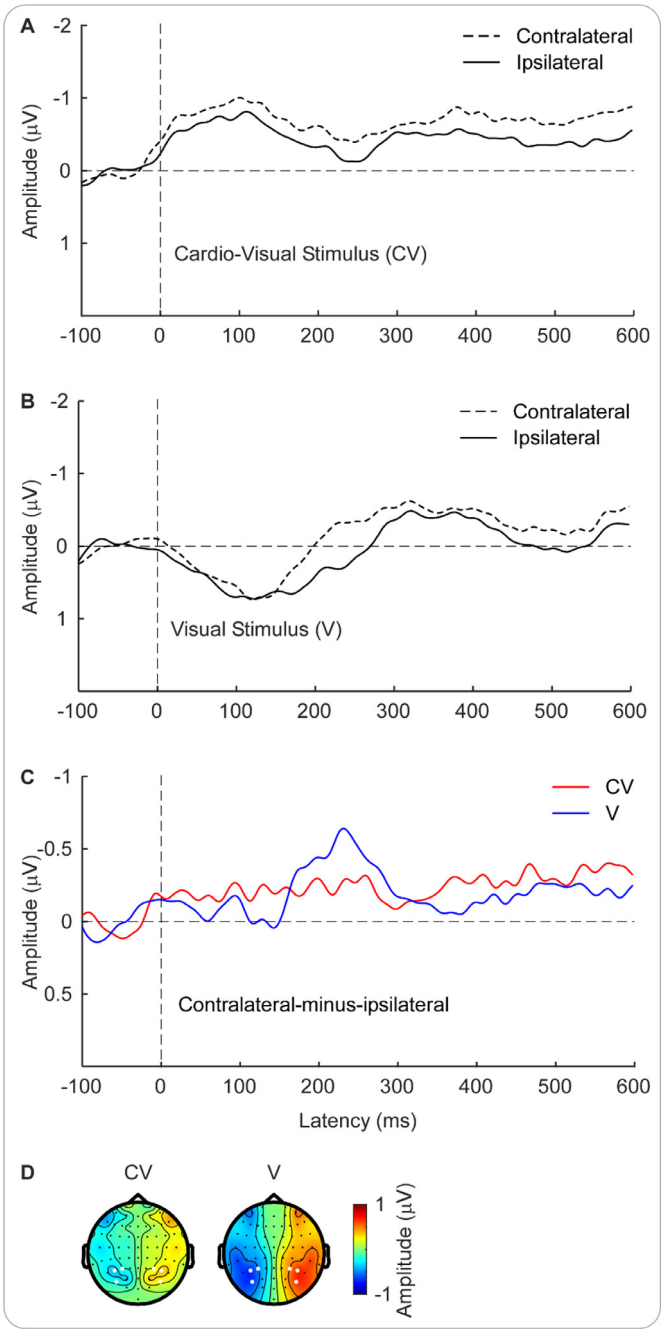

Fig. 4. The effect of cardio-visual integration in lateralized N2pc components. Grand-average waveforms elicited contralateral and ipsilateral to the location of the bimodal cardio-visual stimulus (A) or the unimodal visual stimulus (B). (C) Grand-average contralateral-minus-ipsilateral difference waveforms elicited by the bimodal cardio-visual stimulus and by the unimodal visual stimulus, respectively. Permutation analysis indicated that compared to the unimodal visual stimulus, the bimodal cardio-visual stimulus elicited a lower N2pc amplitude. This corresponded to a cluster extended from 220 to 246 ms after stimulus onset over lateral posterior electrodes. Electrodes with high contribution to the cluster (left hemisphere: P5, PO7, and P3; right hemisphere: P6, PO8, and P4) are highlighted with enlarged white dots in the scalp topographies in (D). The scalp topographies show amplitude differences at homologous electrodes over the hemisphere contralateral and ipsilateral to the target location, with electrodes on the midline artificially set to zero.

bimodal cardio-visual stimulus elicited a lower N2pc amplitude (-0.26 ± 0.07 μV; BF_{10} = 6.06; see Supplementary Fig. 5).

3.5.4. *Time-frequency results based on corrected data*

The nonparametric cluster-based permutation *t*-test for oscillation power revealed a significant cluster within the beta range (13–22 Hz; CP5, P7, P5, PO7, and P4; ~120–300 ms; p = .007, Cohen's d = -0.71). The beta power elicited by the bimodal cardio-visual stimulus (0.49 ± 0.15 dB) was lower than the summed beta power elicited by the unimodal cardiac signals and visual stimulus (0.79 ± 0.17 dB; BF_{10} = 26.71; see Supplementary Fig. 6).

The nonparametric cluster-based permutation *t*-test for lateralized oscillation power revealed a significant cluster within the beta range (16–26 Hz; left hemisphere: P5, PO7, and P3; right hemisphere: P6, PO8, and P4; ~170–360 ms; p = .003, Cohen's d = 1.03). Compared to the unimodal visual stimulus (-0.21 ± 0.04 dB), the bimodal cardio-visual stimulus elicited weaker beta lateralization (0.05 ± 0.04 dB; BF_{10} = 1166.22; see Supplementary Fig. 7).

In summary, our linear regression analyses did not return any linear relationship between the changes in cardiac activity (as measured by ECG amplitude, ECG power, and heart rate) and the effects in early ERP amplitude and early EEG power. More importantly, after correcting for cardiac cycle-related artifacts by subtracting the EEG signal of the resting condition from the EEG signal of task conditions, we observed similar effects based on corrected EEG data as those based on uncorrected EEG data. These results indicate that the observed effects are reflective of neural responses rather than cardiac cycle-related artifacts.

4. Discussion

In this study, we explored the multisensory integration of cardiac signals with a visual target in a dynamic cluttered environment by pairing a dynamic visual search task with an ECG recording. We further recorded EEG to explore brain mechanisms associated with this phenomenon. We observed prolonged reaction times when the color change of the visual target occurred simultaneously with the presence of strong cardiac signals concerning the state of cardiovascular arousal (i.e., presented at the end of ventricular systole), compared to when the color change of the visual target occurred at a time when cardiac arousal was relatively low (i.e., presented at the end of ventricular diastole). This result indicates that the co-occurrence of the target change together with cardiac afferent signals makes it harder to detect the visual target among multiple visual stimuli. Moreover, the co-occurrence of the target change with cardiac signals modulated the ERP responses and the beta power at an early stage (~100 ms after stimulus onset) and suppressed lateralization effects of the N2pc component and the beta-band activity at a later stage (~200 ms after stimulus onset). EEG results hereby reveal distinct periods of electrophysiological modulations that reflect the cardio-visual integration.

The results of the present study are – to the best of our knowledge – the first to demonstrate that multisensory integration of cardiac signals with a visual target negatively affects its detection among multiple visual stimuli. Findings hereby extend earlier reports that simultaneous cardiac signals suppress the perception of a single visual event (McIntyre et al., 2007; Sandman et al., 1977; Walker and Sandman, 1982). Specifically, we observed that searching for the visual target in a dynamically changing visual display took longer when the color change of the visual target coincided with strong cardiac arousal signals compared to when cardiac arousal was relatively weak. Similar perceptual attenuation effects have been reported in other exteroceptive modalities, although based on single events only. For example, auditory stimuli presented at cardiac systole compared with diastole led to prolonged reaction times (Yang et al., 2017) and lower likelihood to be judged as louder (Cohen et al., 1980), indicating that cardiac signals can suppress auditory perception. In addition, in the field of pain and somatosensory perception, participants exhibited higher pain thresholds

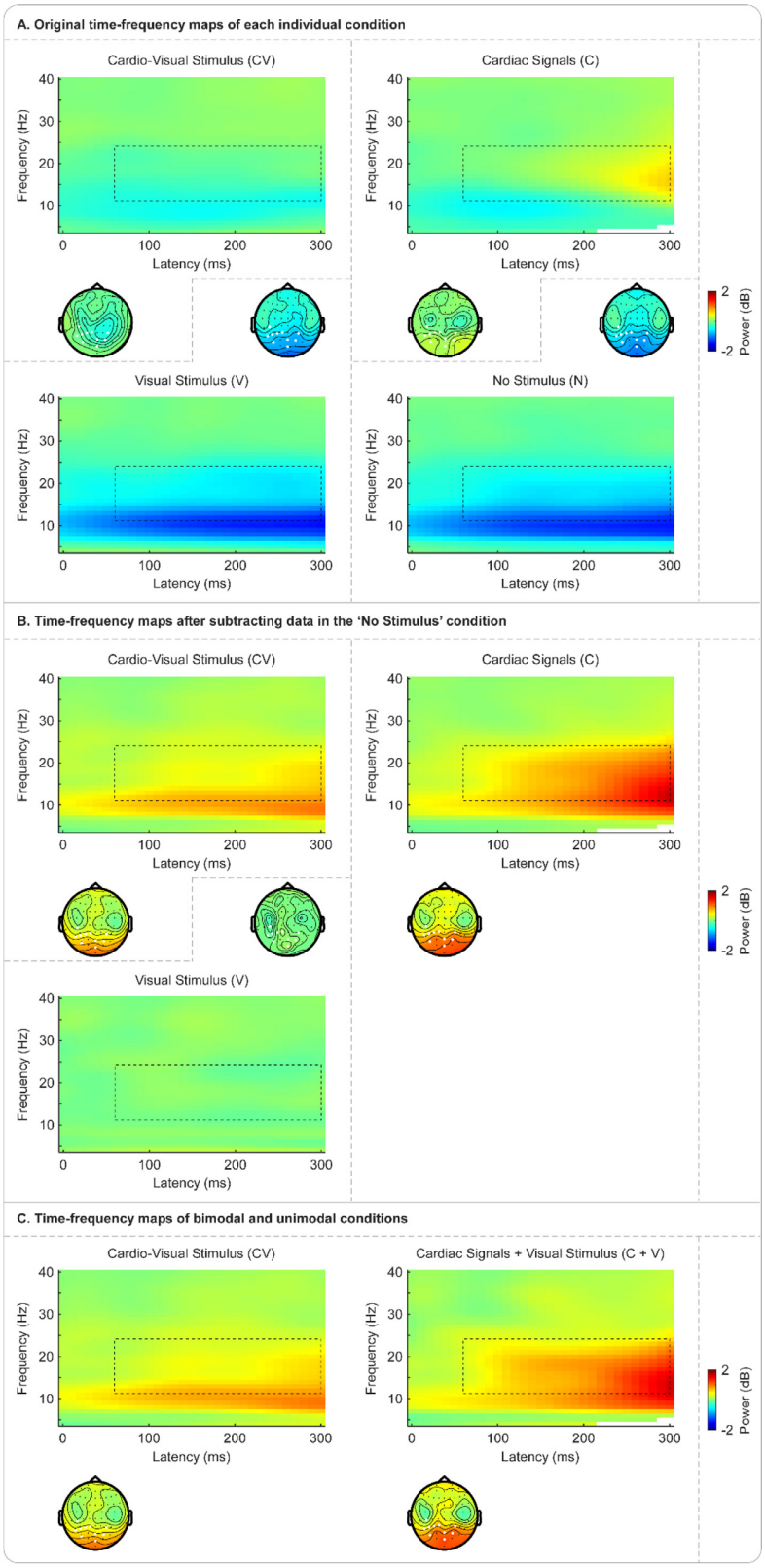

Fig. 5. Early cardio-visual integration in oscillatory power. (A) The original grand-average time-frequency maps elicited by the bimodal cardio-visual stimulus, the unimodal cardiac signals, the unimodal visual stimulus, and the "no stimulus", respectively. (B) The grand-average time-frequency maps elicited by the bimodal cardio-visual stimulus, the unimodal cardiac signals, and the unimodal visual stimulus after subtraction of the time-frequency map elicited by the "no stimulus", respectively. (C) The grand-average time-frequency map elicited by the bimodal cardio-visual stimulus and the summed time-frequency map elicited by the unimodal cardiac signals and visual stimulus. All time-frequency maps were averaged over the posterior electrodes (CP5, P7, P5, P3, P1, PO7, POz, PO4, P4, and Oz) to match the electrodes used in Fig. 3. These electrodes are highlighted with enlarged white dots in the scalp topographies. Permutation analysis indicated that the upper-alpha/beta power elicited by the bimodal cardio-visual stimulus was lower than the summed upper-alpha/beta power elicited by the unimodal cardiac signals and visual stimulus. This corresponded to a cluster extended from 60 to 300 ms after stimulus onset in frequencies from 11 to 24 Hz, marked using dashed rectangles in the time-frequency maps.

(Wilkinson et al., 2013) and worse performance in detecting and localizing somatosensory stimuli during cardiac systole compared to diastole (Al et al., 2020, 2021; Motyka et al., 2019). These studies also support the inhibitory effect of systolic cardiac signals on exteroceptive perception.

More importantly, the present study reveals the brain dynamics underlying this perceptual attenuation phenomenon, which is characterized by electrophysiological modulations during two time periods. First, we observed early modulations in both ERP responses and oscillation power for correctly reported cardio-visual targets. Specifically,

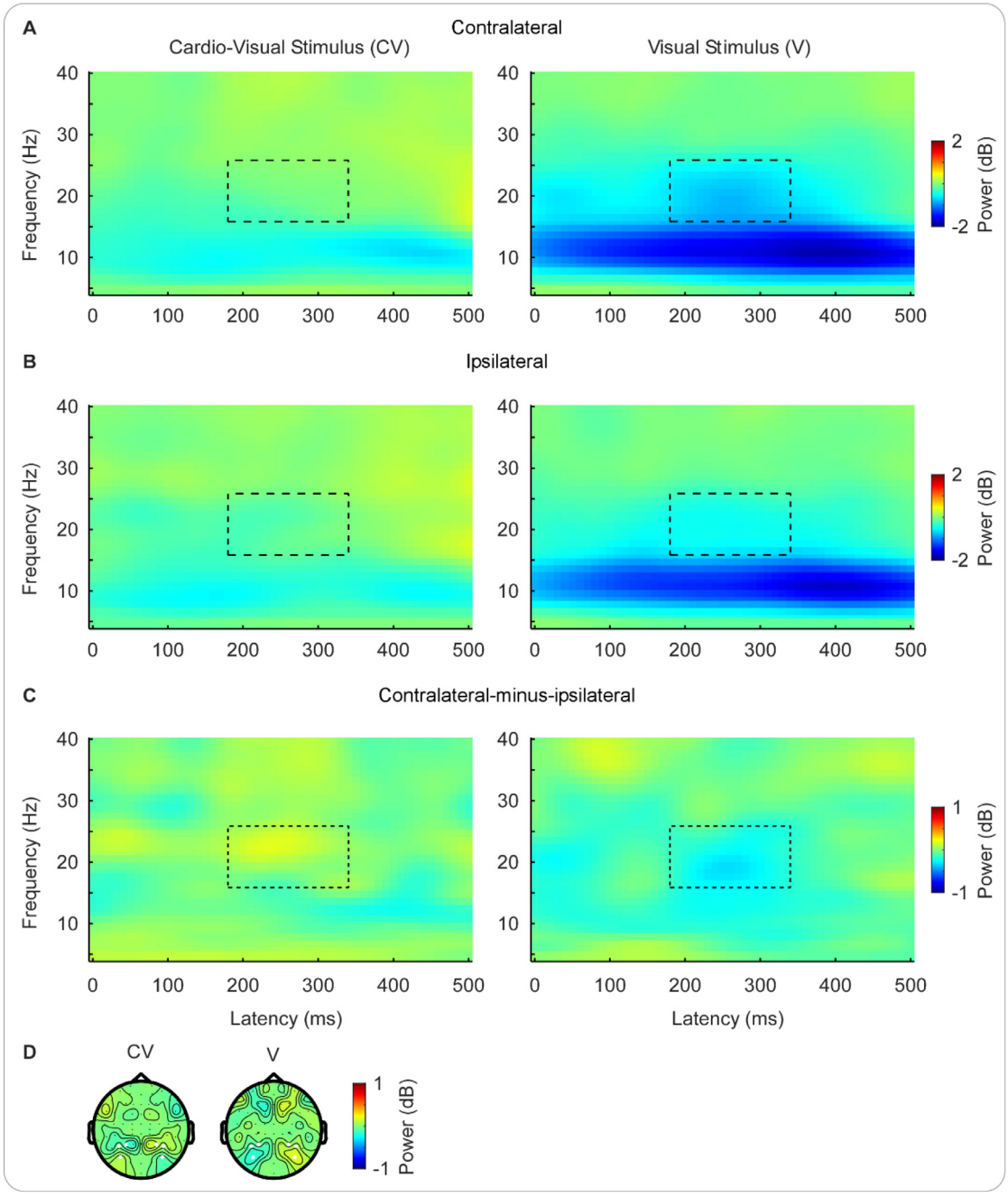

Fig. 6. The effect of cardio-visual integration in lateralized oscillation power. Grand-average time-frequency maps for oscillation power elicited contralateral (A) or ipsilateral (B) to the target location. (C) Grand-average time-frequency maps for contralateral-minus-ipsilateral difference oscillation power. Time-frequency maps elicited by the bimodal cardio-visual stimulus (left panel) and the unimodal visual stimulus (right panel) were averaged over lateral posterior electrodes (left hemisphere: P5, PO7, and P3; right hemisphere: P6, PO8, and P4) respectively to match the electrodes used in Fig. 4. These electrodes are highlighted with enlarged white dots in the scalp topographies in (D). Permutation analysis indicated that compared to the bimodal visual stimulus, the bimodal cardio-visual stimulus elicited weaker beta-band lateralization. This corresponded to a cluster extended from 180 to 340 ms after stimulus onset in frequencies from 16 to 26 Hz, marked using dashed rectangles in the time-frequency maps. The scalp topographies show power differences at homologous electrodes over the hemisphere contralateral and ipsilateral to the target location, with electrodes on the midline artificially set to zero.

the modulation of ERP amplitudes and beta power started at ~90 and ~120 ms respectively, suggesting a rapid interplay between cardiac processing and visual processing. The latencies of these early multisensory responses are consistent with earlier studies reporting cross-modal interactions between different exteroceptive senses. For example, prior studies on auditory-visual (Giard and Peronnet, 1999; Molholm et al., 2002; Senkowski et al., 2011; Van der Burg et al., 2011) and auditory-somatosensory integration (Foxe et al., 2000; Murray et al., 2004) have reported early ERP modulations starting at around 50 ms after stimulus onset. Early modulations in the alpha-/beta-band activity have also been observed to start at around 100 ms after the presentation of the auditory-visual stimulus (Gleiss and Kayser, 2014; Michail et al., 2021). In addition, the parietal-occipital distribution of these early electrophysiological modulations observed in the current study corresponds to claims that the parietal cortex (e.g., inferior parietal lobule) and primary cortices (e.g., primary visual cortex) are involved

in early multisensory integration (Gentile et al., 2010; Murray et al., 2016).

The early ERP modulation seems to be super-additive, i.e., the ERP amplitude elicited by the bimodal cardio-visual stimulus showed increased negativity relative to the summed ERP amplitude elicited by the unimodal cardiac signals and visual stimulus. However, it is difficult to determine the directionality of the cardio-visual interaction simply according to this result, as the polarity of ERP waveforms recorded at scalp surface does not necessarily reflect the directionality of underlying neural activity (Cappe et al., 2010). Interestingly, the association between behavioral improvement and the sub-additive ERP modulation has been well established in the field of auditory-visual integration. For example, studies using animal models have repeatedly reported sub-additive neural response interactions that enhanced sensory processing (Angelaki et al., 2009; Bizley et al., 2007; Kayser et al., 2009). Likewise, many human studies have shown that the behavioral benefits of multisensory stimuli are related to sub-additive ERP responses (Mercier et al., 2013; Stekelenburg and Vroomen, 2012; Van der Burg et al., 2011). Therefore, it is reasonable to speculate that super-additive ERP responses observed in the present study reflect decreased neural responses to the bimodal cardio-visual stimulus. This view was also supported by our finding in oscillation power, i.e., the power elicited by the bimodal cardio-visual stimulus was lower than the summed power elicited by the unimodal cardiac signals and visual stimulus within the upper-alpha/beta range. Specifically, decreased posterior alpha/beta power may suggest that the participants had to deploy increased attentional resources in the bimodal cardio-visual condition in order to detect the target (Kaiser et al., 2022; Sadaghiani and Kleinschmidt, 2016). Therefore, this could represent further evidence that the presence of cardiac signals in combination with visual information inhibited the processing of such sensory input, which participants needed to compensate for probably by increasing their attentional effort. Altogether, these early modulations in ERP responses and oscillation power suggest an inhibitory cardio-visual integration in early sensory processing.

In addition, we also observed reduced ERP responses and oscillation power in a later time window. Specifically, the bimodal cardio-visual compared with the unimodal visual stimulus elicited lower N2pc amplitude (~220–250 ms) and weaker beta lateralization (~170–360 ms). Both lateralized N2pc component and beta activity are known to be modulated by visuospatial selective attention (Bacigalupo and Luck, 2019; Bauer et al., 2012). Larger lateralization effects in N2pc amplitudes and beta power may reflect more attention to the lateralized visual target. Therefore, our findings may indicate that participants paid less attention to external visual information when it coincided with strong cardiac arousal signals compared to when cardiac arousal was relatively weak. However, future studies are needed to clarify the exact mechanisms underlying the effects reported here. The modulation of attentional resources has been repeatedly proposed as the potential mechanism underlying the cardiac cycle effects on exteroception (Al et al., 2020, 2021). Interestingly, a recent study found that participants had more fixations at diastole and more saccades at systole in a free visual search task (Galvez-Pol et al., 2020). Given that people obtain visual information during fixations rather than during saccades (Pertzov et al., 2009), this result suggests that people especially tend to sample task-relevant visual information in the external environment when cardiac signals are relatively weak and in this way may release attentional resources.

Our attentional modulation account may be further explained within the larger framework of predictive coding. Predictive coding implies that perceptual content is determined by knowledge-driven active inference on the causes of sensory signals (Clark, 2013; Friston, 2009), which is applied not only to exteroception but probably also to interoception such as cardiac signals (Seth, 2013). The goal of this active inference is to minimize prediction error (Friston et al., 2017). Cardiac interoceptive information is conveyed to the brain mainly via the firing of arterial baroreceptors during the systolic phase of each cardiac cycle (Azzalini et al., 2019; Garfinkel and Critchley, 2016). This periodical transmission of cardiac signals is predictable and therefore attenuated by the brain to reduce the possibility of mistaking these internal spontaneous signals as external input (Barrett and Simmons, 2015; Seth and Friston, 2016). In the present study, the external target change occurring at cardiac systole compared with diastole may be more likely to be regarded as heartbeat-related, task-irrelevant “internal noise”, and thus obtain less attentional and representational resources, finally leading to impaired visual search. Such a predictive coding mechanism has also been proposed to explain the suppression of somatosensory-evoked potentials and pain-evoked potentials during cardiac systole compared to diastole (Al et al., 2020, 2021; Gray et al., 2010), as well as the attenuation of auditory-evoked potentials for heartbeat-related sounds relative to externally generated sounds (van Elk et al., 2014).

In conclusion, multisensory integration of systolic cardiac signals with visual stimulation disrupted the detection of a goal-relevant target among multiple visual distractors, as reflected by prolonged reaction times as well as inhibitory modulations in ERP amplitudes and oscillation power during both early and late time periods. The possible mechanisms underlying this heart-brain interaction are the attenuation of early sensory processing and the reduction of attentional resources deployed toward the outer visual target. Our findings highlight the role of cardiac information in visual processing and further our understanding of the brain dynamics underlying multisensory perception involving both interoception and exteroception.

Funding

This work was supported by Deutsche Forschungsgemeinschaft [SCHU 2471/5-1 to S.S-B.] and China Scholarship Council [grant number 202004910347 to Q.R.].

Declaration of Competing Interest

None.

Credit authorship contribution statement

Qiaoyue Ren: Conceptualization, Methodology, Investigation, Data curation, Formal analysis, Visualization, Writing – original draft. **Amanda C. Marshall:** Methodology, Writing – review & editing. **Jakob Kaiser:** Methodology, Writing – review & editing. **Simone Schütz-Bosbach:** Conceptualization, Methodology, Writing – review & editing, Supervision, Funding acquisition.

Data Availability

I have shared the link to my data/code at the attach file step.

Acknowledgments

We thank Elsa Sangaran and Sara-Estelle Gößwein for their assistance in data collection.

Supplementary materials

Supplementary material associated with this article can be found, in the online version, at doi:10.1016/j.neuroimage.2022.119549.

References

Adelhöfer, N., Schreiter, M.L., Beste, C., 2020. Cardiac cycle gated cognitive-emotional control in superior frontal cortices. NeuroImage 222, 117275. doi:10.1016/j.neuroimage.2020.117275.

Al, E., Iliopoulos, F., Forschack, N., Nierhaus, T., Grund, M., Motyka, P., Villringer, A., 2020. Heart-brain interactions shape somatosensory perception and evoked potentials. Proc. Natl. Acad. Sci. U. S. A. 117 (19), 10575–10584. doi:10.1073/pnas.1915629117.

Al, E., Iliopoulos, F., Nikulin, V.V., Villringer, A., 2021. Heartbeat and somatosensory perception. NeuroImage 238, 118247. doi:10.1016/j.neuroimage.2021.118247.
Angelaki, D.E., Gu, Y., DeAngelis, G.C., 2009. Multisensory integration: psychophysics, neurophysiology, and computation. Curr. Opin. Neurobiol. 19 (4), 452–458. doi:10.1016/j.conb.2009.06.008.
Arslanova, I., Galvez-Pol, A., Calvo-Merino, B., Forster, B., 2019. Searching for bodies: ERP evidence for independent somatosensory processing during visual search for body-related information. NeuroImage 195, 140–149. doi:10.1016/j.neuroimage.2019.03.037.
Azzalini, D., Rebollo, I., Tallon-Baudry, C., 2019. Visceral signals shape brain dynamics and cognition. Trends Cogn. Sci. 23 (6), 488–509. doi:10.1016/j.tics.2019.03.007.
Bacigalupo, F., Luck, S.J., 2019. Lateralized suppression of alpha-band EEG activity as a mechanism of target processing. J. Neurosci. 39 (5), 900–917. doi:10.1523/JNEUROSCI.0183-18.2018.
Barrett, L.F., Simmons, W.K., 2015. Interoceptive predictions in the brain. Nat. Rev. Neurosci. 16 (7), 419–429. doi:10.1038/nrn3950.
Bauer, M., Kluge, C., Bach, D., Bradbury, D., Heinze, H.J., Dolan, R.J., Driver, J., 2012. Cholinergic enhancement of visual attention and neural oscillations in the human brain. Curr. Biol. 22 (5), 397–402. doi:10.1016/j.cub.2012.01.022.
Bizley, J.K., Nodal, F.R., Bajo, V.M., Nelken, I., King, A.J., 2007. Physiological and anatomical evidence for multisensory interactions in auditory cortex. Cereb. Cortex 17 (9), 2172–2189. doi:10.1093/cercor/bhl128.
Cappe, C., Thut, G., Romei, V., Murray, M.M., 2010. Auditory–visual multisensory interactions in humans: timing, topography, directionality, and sources. J. Neurosci. 30 (38), 12572–12580. doi:10.1523/JNEUROSCI.1099-10.2010.
Chen, W.G., Schloesser, D., Arensdorf, A.M., Simmons, J.M., Cui, C., Valentino, R., Langevin, H.M., 2021. The emerging science of interoception: sensing, integrating, interpreting, and regulating signals within the self. Trends Neurosci. 44 (1), 3–16. doi:10.1016/j.tins.2020.10.007.
Clark, A., 2013. Whatever next? Predictive brains, situated agents, and the future of cognitive science. Behav. Brain Sci. 36 (3), 181–204. doi:10.1017/S0140525X12000477.
Cohen, R., Lieb, H., Rist, F., 1980. Loudness judgments, evoked potentials, and reaction time to acoustic stimuli early and late in the cardiac cycle in chronic schizophrenics. Psychiatry Res. 3 (1), 23–29. doi:10.1016/0165-1781(80)90044-X.
Coll, M.P., Hobson, H., Bird, G., Murphy, J., 2021. Systematic review and meta-analysis of the relationship between the heartbeat-evoked potential and interoception. Neurosci. Biobehav. Rev. 122, 190–200. doi:10.1016/j.neubiorev.2020.12.012.
DeSaix, P., Betts, J.G., Johnson, E., Johnson, J.E., Korol, O., Kruse, D.H., Poe, B., Wise, J.A., Young, K.A., 2018. Anatomy & Physiology: OpenStax. 12th Media Services (18 May 2016).
Elliott, R., Graf, V., 1972. Visual sensitivity as a function of phase of cardiac cycle. Psychophysiology 9 (3), 357–361. doi:10.1111/j.1469-8986.1972.tb03219.x.
Fong, C.Y., Law, W.H.C., Braithwaite, J.J., Mazaheri, A., 2020. Differences in early and late pattern-onset visual-evoked potentials between self-reported migraineurs and controls. NeuroImage Clin. 25, 102122. doi:10.1016/j.nicl.2019.102122.
Foxe, J.J., Morocz, I.A., Murray, M.M., Higgins, B.A., Javitt, D.C., Schroeder, C.E., 2000. Multisensory auditory–somatosensory interactions in early cortical processing revealed by high-density electrical mapping. Cogn. Brain Res. 10 (1), 77–83. doi:10.1016/S0926-6410(00)00024-0.
Friston, K., 2009. The free-energy principle: a rough guide to the brain? Trends Cogn. Sci. 13 (7), 293–301. doi:10.1016/j.tics.2009.04.005.
Friston, K., FitzGerald, T., Rigoli, F., Schwartenbeck, P., Pezzulo, G., 2017. Active inference: a process theory. Neural Comput. 29 (1), 1–49. doi:10.1162/NECO_a_00912.
Galvez-Pol, A., McConnell, R., Kilner, J.M., 2020. Active sampling in visual search is coupled to the cardiac cycle. Cognition 196, 104149. doi:10.1016/j.cognition.2019.104149.
Garfinkel, S.N., Critchley, H.D., 2016. Threat and the body: how the heart supports fear processing. Trends Cogn. Sci. 20 (1), 34–46. doi:10.1016/j.tics.2015.10.005.
Garfinkel, S.N., Minati, L., Gray, M.A., Seth, A.K., Dolan, R.J., Critchley, H.D., 2014. Fear from the heart: sensitivity to fear stimuli depends on individual heartbeats. J. Neurosci. 34 (19), 6573–6582. doi:10.1523/JNEUROSCI.3507-13.2014.
Gentile, G., Petkova, V.I., Ehrsson, H.H., 2010. Integration of visual and tactile signals from the hand in the human brain: an fmri study. J. Neurophysiol. 105 (2), 910–922. doi:10.1152/jn.00840.2010.
Giard, M.H., Peronnet, F., 1999. Auditory-visual integration during multimodal object recognition in humans: a behavioral and electrophysiological study. J. Cogn. Neurosci. 11 (5), 473–490. doi:10.1162/089892999563544.
Gleiss, S., Kayser, C., 2014. Oscillatory mechanisms underlying the enhancement of visual motion perception by multisensory congruency. Neuropsychologia 53, 84–93. doi:10.1016/j.neuropsychologia.2013.11.005.
Gray, M.A., Minati, L., Paoletti, G., Critchley, H.D., 2010. Baroreceptor activation attenuates attentional effects on pain-evoked potentials. Pain 151 (3), 853–861. doi:10.1016/j.pain.2010.09.028.
Hu, L., Zhang, Z., 2019. EEG Signal Processing and Feature Extraction. Springer.
JASP Team, 2022. JASP (Version 0.16.3) [Computer software]. https://jasp-stats.org/.
Kaiser, J., Iliopoulos, P., Steinmassl, K., Schütz-Bosbach, S., 2022. Preparing for success: neural frontal theta and posterior alpha dynamics during action preparation predict flexible resolution of cognitive conflicts. J. Cogn. Neurosci. 34 (6), 1070–1089. doi:10.1162/jocn_a_01846.
Kaiser, J., Schütz-Bosbach, S., 2021. Motor interference, but not sensory interference, increases midfrontal theta activity and brain synchronization during reactive control. J. Cogn. Neurosci. 41 (8), 1788–1801. doi:10.1523/JNEUROSCI.1682-20.2020.
Kayser, C., Petkov, C.I., Logothetis, N.K., 2009. Multisensory interactions in primate auditory cortex: fMRI and electrophysiology. Hear. Res. 258 (1), 80–88. doi:10.1016/j.heares.2009.02.011.
Kayser, S.J., Philiastides, M.G., Kayser, C., 2017. Sounds facilitate visual motion discrimination via the enhancement of late occipital visual representations. NeuroImage 148, 31–41. doi:10.1016/j.neuroimage.2017.01.010.
Kern, M., Aertsen, A., Schulze-Bonhage, A., Ball, T., 2013. Heart cycle-related effects on event-related potentials, spectral power changes, and connectivity patterns in the human ECoG. NeuroImage 81, 178–190. doi:10.1016/j.neuroimage.2013.05.042.
Leo, F., Bertini, C., di Pellegrino, G., Làdavas, E., 2008. Multisensory integration for orienting responses in humans requires the activation of the superior colliculus. Exp. Brain Res. 186 (1), 67–77. doi:10.1007/s00221-007-1204-9.
Luck, S.J., Hillyard, S.A., 1994. Electrophysiological correlates of feature analysis during visual search. J. Exp. Psychol. Hum. Percept. Perform. 31 (3), 291–308. doi:10.1111/j.1469-8986.1994.tb02218.x.
Makowski, D., Pham, T., Lau, Z.J., Brammer, J.C., Lespinasse, F., Pham, H., Chen, S.H.A., 2021. NeuroKit2: a Python toolbox for neurophysiological signal processing. Behav. Res. Methods 53 (4), 1689–1696. doi:10.3758/s13428-020-01516-y.
Maris, E., Oostenveld, R., 2007. Nonparametric statistical testing of EEG-and MEG-data. J. Neurosci. Methods 164 (1), 177–190. doi:10.1016/j.jneumeth.2007.03.024.
Marshall, A.C., Gentsch-Ebrahimzadeh, A., Schütz-Bosbach, S., 2022. From the inside out: interoceptive feedback facilitates the integration of visceral signals for efficient sensory processing. NeuroImage 251, 119011. doi:10.1016/j.neuroimage.2022.119011.
Martuzzi, R., Murray, M.M., Michel, C.M., Thiran, J.P., Maeder, P.P., Clarke, S., Meuli, R.A., 2007. Multisensory interactions within human primary cortices revealed by BOLD dynamics. Cereb. Cortex 17 (7), 1672–1679. doi:10.1093/cercor/bhl077.
McIntyre, D., Ring, C., Hamer, M., Carroll, D., 2007. Effects of arterial and cardiopulmonary baroreceptor activation on simple and choice reaction times. Psychophysiology 44 (6), 874–879. doi:10.1111/j.1469-8986.2007.00547.x.
Mercier, M.R., Foxe, J.J., Fiebelkorn, I.C., Butler, J.S., Schwartz, T.H., Molholm, S., 2013. Auditory-driven phase reset in visual cortex: human electrocorticography reveals mechanisms of early multisensory integration. NeuroImage 79, 19–29. doi:10.1016/j.neuroimage.2013.04.060.
Michail, G., Senkowski, D., Holtkamp, M., Wächter, B., Schroeder, C.E., Keil, J., 2021. Early beta oscillations in multisensory association areas underlie crossmodal performance enhancement. bioRxiv. NeuroImage doi:10.1016/j.neuroimage.2022.119307.
Molholm, S., Ritter, W., Murray, M.M., Javitt, D.C., Schroeder, C.E., Foxe, J.J., 2002. Multisensory auditory–visual interactions during early sensory processing in humans: a high-density electrical mapping study. Cogn. Brain Res. 14 (1), 115–128. doi:10.1016/S0926-6410(02)00066-6.
Motyka, P., Grund, M., Forschack, N., Al, E., Villringer, A., Gaebler, M., 2019. Interactions between cardiac activity and conscious somatosensory perception. Psychophysiology 56 (10), e13424. doi:10.1111/psyp.13424.
Murray, M.M., Molholm, S., Michel, C.M., Heslenfeld, D.J., Ritter, W., Javitt, D.C., Foxe, J.J., 2004. Grabbing your ear: rapid auditory–somatosensory multisensory interactions in low-level sensory cortices are not constrained by stimulus alignment. Cereb. Cortex 15 (7), 963–974. doi:10.1093/cercor/bhh197.
Murray, M.M., Thelen, A., Thut, G., Romei, V., Martuzzi, R., Matusz, P.J., 2016. The multisensory function of the human primary visual cortex. Neuropsychologia 83, 161–169. doi:10.1016/j.neuropsychologia.2015.08.011.
Noesselt, T., Bergmann, D., Hake, M., Heinze, H.J., Fendrich, R., 2008. Sound increases the saliency of visual events. Brain Res. 1220, 157–163. doi:10.1016/j.brainres.2007.12.060.
Oostenveld, R., Fries, P., Maris, E., Schoffelen, J.M., 2011. FieldTrip: open source software for advanced analysis of MEG, EEG, and invasive electrophysiological data. Comput. Intell. Neurosci. 2011, 156869. doi:10.1155/2011/156869.
Park, H.D., Bernasconi, F., Salomon, R., Tallon-Baudry, C., Spinelli, L., Seeck, M., Blanke, O., 2018. Neural sources and underlying mechanisms of neural responses to heartbeats, and their role in bodily self-consciousness: an intracranial EEG study. Cereb. Cortex 28 (7), 2351–2364. doi:10.1093/cercor/bhx136.
Park, H.D., Blanke, O., 2019. Heartbeat-evoked cortical responses: underlying mechanisms, functional roles, and methodological considerations. NeuroImage 197, 502–511. doi:10.1016/j.neuroimage.2019.04.081.
Park, H.D., Correia, S., Ducorps, A., Tallon-Baudry, C., 2014. Spontaneous fluctuations in neural responses to heartbeats predict visual detection. Nat. Neurosci. 17 (4), 612–618. doi:10.1038/nn.3671.
Pertzov, Y., Avidan, G., Zohary, E., 2009. Accumulation of visual information across multiple fixations. J. Vis. 9 (10), 2. doi:10.1167/9.10.2.
Petzschner, F.H., Weber, L.A., Wellstein, K.V., Paolini, G., Do, C.T., Stephan, K.E., 2019. Focus of attention modulates the heartbeat evoked potential. NeuroImage 186, 595–606. doi:10.1016/j.neuroimage.2018.11.037.
Pramme, L., Larra, M.F., Schächinger, H., Frings, C., 2014. Cardiac cycle time effects on mask inhibition. Biol. Psychol. 100, 115–121. doi:10.1016/j.biopsycho.2014.05.008.
Pramme, L., Larra, M.F., Schächinger, H., Frings, C., 2016. Cardiac cycle time effects on selection efficiency in vision. Psychophysiology 53 (11), 1702–1711. doi:10.1111/psyp.12728.
Quigley, K.S., Kanoski, S., Grill, W.M., Barrett, L.F., Tsakiris, M., 2021. Functions of interoception: from energy regulation to experience of the self. Trends Neurosci. 44 (1), 29–38. doi:10.1016/j.tins.2020.09.008.
Rae, C.L., Ahmad, A., Larsson, D.E.O., Silva, M., Praag, C.D.G.V., Garfinkel, S.N., Critchley, H.D., 2020. Impact of cardiac interoception cues and confidence on voluntary decisions to make or withhold action in an intentional inhibition task. Sci. Rep. 10, 4184. doi:10.1038/s41598-020-60405-8.
Rae, C.L., Botan, V.E., Gould van Praag, C.D., Herman, A.M., Nyyssönen, J.A., Watson, D.R., Critchley, H.D., 2018. Response inhibition on the stop signal task improves during cardiac contraction. Sci. Rep. 8, 9136. doi:10.1038/s41598-018-27513-y.
Ronchi, R., Bernasconi, F., Pfeiffer, C., Bello-Ruiz, J., Kaliuzhna, M., Blanke, O., 2017. Interoceptive signals impact visual processing: cardiac modulation of visual body perception. NeuroImage 158, 176–185. doi:10.1016/j.neuroimage.2017.06.064.

Sadaghiani, S., Kleinschmidt, A., 2016. Brain networks and α-oscillations: structural and functional foundations of cognitive control. Trends Cogn. Sci. 20 (11), 805–817. doi:10.1016/j.tics.2016.09.004.

Salomon, R., Ronchi, R., Dönz, J., Bello-Ruiz, J., Herbelin, B., Faivre, N., Blanke, O., 2018. Insula mediates heartbeat related effects on visual consciousness. Cortex 101, 87–95. doi:10.1016/j.cortex.2018.01.005.

Salomon, R., Ronchi, R., Dönz, J., Bello-Ruiz, J., Herbelin, B., Martet, R., Blanke, O., 2016. The insula mediates access to awareness of visual stimuli presented synchronously to the heartbeat. J. Neurosci. 36 (18), 5115–5127. doi:10.1523/JNEUROSCI.4262-15.2016.

Sandman, C.A., McCanne, T.R., Kaiser, D.N., Diamond, B., 1977. Heart rate and cardiac phase influences on visual perception. J. Comp. Physiol. Psychol. 91 (1), 189–202. doi:10.1037/h0077302.

Sel, A., Azevedo, R.T., Tsakiris, M., 2017. Heartfelt self: cardio-visual integration affects self-face recognition and interoceptive cortical processing. Cereb. Cortex 27 (11), 5144–5155. doi:10.1093/cercor/bhw296/J.Cerebral.Cortex.

Senkowski, D., Saint-Amour, D., Höfle, M., Foxe, J.J., 2011. Multisensory interactions in early evoked brain activity follow the principle of inverse effectiveness. NeuroImage 56 (4), 2200–2208. doi:10.1016/j.neuroimage.2011.03.075.

Seth, A.K., 2013. Interoceptive inference, emotion, and the embodied self. Trends Cogn. Sci. 17 (11), 565–573. doi:10.1016/j.tics.2013.09.007.

Seth, A.K., Friston, K.J., 2016. Active interoceptive inference and the emotional brain. Philos. Trans. R. Soc. B Biol. Sci. 371 (1708), 20160007. doi:10.1098/rstb.2016.0007.

Stekelenburg, J.J., Vroomen, J., 2012. Electrophysiological correlates of predictive coding of auditory location in the perception of natural audiovisual events. Front. Integr. Neurosci. 6, 26. doi:10.3389/fnint.2012.00026.

Tallon-Baudry, C., Bertrand, O., 1999. Oscillatory gamma activity in humans and its role in object representation. Trends Cogn. Sci. 3 (4), 151–162. doi:10.1016/S1364-6613(99)01299-1.

Talsma, D., Woldorff, M.G., 2005. Selective attention and multisensory integration: multiple phases of effects on the evoked brain activity. J. Cogn. Neurosci. 17 (7), 1098–1114. doi:10.1162/0898929054475172.

Tang, X., Wu, J., Shen, Y., 2016. The interactions of multisensory integration with endogenous and exogenous attention. Neurosci. Biobehav. Rev. 61, 208–224. doi:10.1016/j.neubiorev.2015.11.002.

van Atteveldt, N., Murray, M.M., Thut, G., Schroeder, C.E., 2014. Multisensory integration: flexible use of general operations. Neuron 81 (6), 1240–1253. doi:10.1016/j.neuron.2014.02.044.

Van der Burg, E., Olivers, C.N., Bronkhorst, A.W., Theeuwes, J., 2008. Pip and pop: nonspatial auditory signals improve spatial visual search. J. Exp. Psychol. Hum. Percept. Perform. 34 (5), 1053. doi:10.1037/0096-1523.34.5.1053.

Van der Burg, E., Talsma, D., Olivers, C.N., Hickey, C., Theeuwes, J., 2011. Early multisensory interactions affect the competition among multiple visual objects. NeuroImage 55 (3), 1208–1218. doi:10.1016/j.neuroimage.2010.12.068.

van Elk, M., Lenggenhager, B., Heydrich, L., Blanke, O., 2014. Suppression of the auditory N1-component for heartbeat-related sounds reflects interoceptive predictive coding. Biol. Psychol. 99, 172–182. doi:10.1016/j.biopsycho.2014.03.004.

Viola, F.C., Thorne, J., Edmonds, B., Schneider, T., Eichele, T., Debener, S., 2009. Semi-automatic identification of independent components representing EEG artifact. Clin. Neurophysiol. 120 (5), 868–877. doi:10.1016/j.clinph.2009.01.015.

Wagenmakers, E.J., Love, J., Marsman, M., Jamil, T., Ly, A., Verhagen, J., Morey, R.D., 2018. Bayesian inference for psychology. Part II: example applications with JASP. Psychon. Bull. Rev. 25 (1), 58–76. doi:10.3758/s13423-017-1323-7.

Wagenmakers, E.J., Marsman, M., Jamil, T., Ly, A., Verhagen, J., Love, J., Morey, R.D., 2018. Bayesian inference for psychology. Part I: theoretical advantages and practical ramifications. Psychon. Bull. Rev. 25 (1), 35–57. doi:10.3758/s13423-017-1343-3.

Walker, B.B., Sandman, C.A., 1982. Visual evoked potentials change as heart rate and carotid pressure change. Psychophysiology 19 (5), 520–527. doi:10.1111/j.1469-8986.1982.tb02579.x.

Wallace, M.T., Woynaroski, T.G., Stevenson, R.A., 2020. Multisensory integration as a window into orderly and disrupted cognition and communication. Annu. Rev. Psychol. 71 (1), 193–219. doi:10.1146/annurev-psych-010419-051112.

Wilkinson, M., McIntyre, D., Edwards, L., 2013. Electrocutaneous pain thresholds are higher during systole than diastole. Biol. Psychol. 94 (1), 71–73. doi:10.1016/j.biopsycho.2013.05.002.

Yang, X., Jennings, J.R., Friedman, B.H., 2017. Exteroceptive stimuli override interoceptive state in reaction time control. Psychophysiology 54 (12), 1940–1950. doi:10.1111/psyp.12958.

Zhang, L., Li, Z., Zhang, F., Gu, R., Peng, W., Hu, L., 2020. Demystifying signal processing techniques to extract task-related EEG responses for psychologists. Brain Sci. Adv. 6 (3), 171–188. doi:10.26599/BSA.2020.9050018.

Zhao, S., Wang, Y., Feng, C., Feng, W., 2020. Multiple phases of cross-sensory interactions associated with the audiovisual bounce-inducing effect. Biol. Psychol. 149, 107805. doi:10.1016/j.biopsycho.2019.107805.

Zhao, S., Wang, Y., Xu, H., Feng, C., Feng, W., 2018. Early cross-modal interactions underlie the audiovisual bounce-inducing effect. NeuroImage 174, 208–218. doi:10.1016/j.neuroimage.2018.03.036.